Ductilizing Bulk Metallic Glass Composite by Tailoring Stacking Fault Energy

Y. Wu,[1] D. Q. Zhou,[1] W. L. Song,[1] H. Wang,[1] Z. Y. Zhang,[1] D. Ma,[2] X. L. Wang,[3] and Z. P. Lu[1,*]

[1]*State Key Laboratory for Advanced Metals and Materials, University of Science and Technology Beijing, Beijing 100083, China*

[2]*Neutron Scattering Science Division, Oak Ridge National Laboratory, Oak Ridge, Tennessee 37831, USA*

[3]*Department of Physics and Materials Science, City University of Hong Kong, Hong Kong, China*

(Received 17 January 2012; published 14 December 2012)

Martensitic transformation was successfully introduced to bulk metallic glasses as the reinforcement micromechanism. In this Letter, it was found that the twinning property of the reinforcing crystals can be dramatically improved by reducing the stacking fault energy through microalloying, which effectively alters the electron charge density redistribution on the slipping plane. The enhanced twinning propensity promotes the martensitic transformation of the reinforcing austenite and, consequently, improves plastic stability and the macroscopic tensile ductility. In addition, a general rule to identify effective microalloying elements based on their electronegativity and atomic size was proposed.

DOI: 10.1103/PhysRevLett.109.245506 PACS numbers: 81.05.Kf, 64.70.pe, 81.30.Kf

Localized shear banding instead of dislocation is the main carrier of plastic deformation in bulk metallic glasses (BMGs) due to their long-range disordering structure [1–4]. The localized deformation mode results in room-temperature brittleness and strain softening, which became a stumbling block for practical applications of BMGs. The above challenge has been addressed in recent years via development of BMG composites consisting of soft reinforcing crystalline phases *in situ* precipitated in the glassy matrix [5,6]. In particular, (CuZr)- and Ti-based BMG composites with austenitic precipitates, which undergo the martensitic transformation upon straining, have shown not only to produce a uniform tensile ductility but also alleviate strain-softening behavior [7–10], which opens up a promising and innovative route for developing high-performance BMGs as engineering materials [11].

Recently, it was suggested that the deformation induced martensitic transformation of the austenitic $B2$-CuZr precipitates in certain BMG composites occurred trough twinning [12,13]. Deformation twinning is an important mode of strain energy relaxation in crystalline metals and also a dominant carrier of plasticity in nanocrystalline metals. In fact, improved mechanical performance has been achieved by tailoring the capability of deformation twinning in nanocrystalline metals [14–17]. The extension and enabling of deformation twinning in BMG composites containing austenitic particles is anticipated to enhance the damage tolerance and mechanical performance of the BMG composites. Thus, a basic understanding of interplay of the plasticity-induced martensitic transformation and deformation twinning in the reinforcing crystals and their contribution to the overall mechanical properties of the current BMG composite are both scientifically and technologically of great interest.

In this Letter, we make an attempt to establish a guideline to improve the propensity of deformation twinning in the reinforced crystals in BMG composites by tailoring the stacking fault energy of the primary slip system with minor alloying addition. The current work suggests that manipulation of the deformation twinning of the crystalline phase in the BMG composites is a feasible approach to ductilizing BMG materials for engineering applications.

Ab initio calculations were based on the density function theory implemented in the Vienna *ab initio* simulation package (VASP) [18,19]. The projector augmented wave basis pseudopotentials [20,21] and the generalized gradient approximation of Perdew and Wang were used for the exchange correlation energy function [22]. Charge density distribution mapping was conducted using a three-dimensional visualization system for electronic and structure analysis [23,24]. The Brillouin zone integrations were performed using Monkhorst-Pack k-point meshes. The stacking fault structure (SFE) was constructed by shifting the top half-layers with a distance u along b (b is partial Burgers vector corresponding to each slip system) [25]. To eliminate the free surface effect on the computed SFE, tests with different slab thicknesses in the range of 6 to 24 layers were conducted and it was determined that 12 layers gave a convergence of 0.001 $\mathrm{J/m^2}$ in the SFE. A 15 Å vacuum gap was added above the supercell to avoid interactions with periodic images [26]. A total energy convergence of 1 meV per atom was obtained with the above configuration and a 460 eV kinetic-energy cutoff.

Alloys with a nominal composition of $Zr_{48}Cu_{48-x}Al_4M_x$ ($x = 0$–2 at.%, M = Co, Ti, Fe, Ni, Ta, Cr, Ga, Hf, Nb, Ta, and Ag) were prepared by arc melting a mixture of constituent elements with a purity of above 99.9% in a Ti-gettered argon atmosphere. The alloy ingots were melted six times to ensure compositional homogeneity. Cylinder samples with a diameter of 3 mm were fabricated by suction casting using copper molds. Structure nature of the as-cast rods was examined by x-ray diffraction and a

JEM 2010F transmission electron microscopy with a field emission gun. Longitudinal and cross section surfaces of the as-cast and strained samples were examined in a ZEISS SUPRA 55 scanning electron microscope (SEM). Tensile tests were carried out in a WDW-200D machine with a maximum load of 200 kN at an engineering strain rate of 2×10^{-4} s^{-1}, and a strain gauge was used to calibrate and directly measure the strain during loading. The onset temperature and activation energy of the martensitic transformation was measured by differential scanning calorimetry (DSC) at a cooling rate ranging from 5 to 20 K/s.

The stacking fault energy, which represents the energy cost per unit area incurred by relative displacement of two parts of a crystal through a shift vector across a certain slip plane, governs the deformation twinning event [27,28]. For the bcc $B2$-CuZr phase, we performed the *ab initio* calculations of the SFE by rigidly shifting the lattice across the {100}, {110}, and {111} planes at an interval of $0.1a$ along the possible slip directions, where a is the $B2$-CuZr lattice constant. Details of the calculation can be found elsewhere [29]. Among all possible lattice planes investigated, the minimum SFE occurred along the (011)[100] slip system, which corresponds to the most favorable slip direction. Subsequently, the SFE as a function of the shift vector along the (011)[100] slip system in the $B2$-CuZr structure with or without half of Cu/Zr atoms on the slipping plane substituted by the other transitional metals was calculated and the results for the Co and Ti substitution of Cu were particularly shown in Fig. 1(a), in comparison with that of the base $B2$-CuZr phase. The SFE value of the stoichiometric CuZr phase shows a maximum of 381 mJ/m^2 at $a/2$, which corresponds to the energy barrier for the stacking fault formation. The addition of Co dramatically reduces the SFE to 75 mJ/m^2, but the substitution of Ti significantly increases the SFE to 445 mJ/m^2. With half of Cu on the (011)[100] slip plane replaced by the other transition metal elements, the maximum value significantly varies from the minimum of 75 mJ/m^2 for Co to the 595 mJ/m^2 for Nb (Fig. 1(b)). This result reveals that alloying additions can produce a dramatic effect on the SFE. It should be pointed out that the doped transitional metals primarily substitute the Cu sites in the $B2$-CuZr structure based on our calculation. When the aforementioned elements replace the Zr sites, on the other hand, the potential energy of the system sharply increases, thereby not energetically favorable.

As proposed by Ogata *et al.* [30,31], variation of the SFE usually has its origins in the electronic structures, and particularly relate to the charge density change during the stacking fault formation. The electronic charge density redistribution, $\Delta\bar{\rho}$, can be obtained by comparing the electronic charge density of the bonding in the faulted structure with that in the initial perfect $B2$ structure on the slipping plane (an example of the comparison can be found in Fig. S1 of the Supplemental Material, see Ref. [32]). Figure 2 shows the SFE values of the $B2$-CuZr phase doped with different alloying elements as a function of the electronic density charge redistribution on the (011)[100] slip system. It can be seen that the doped element

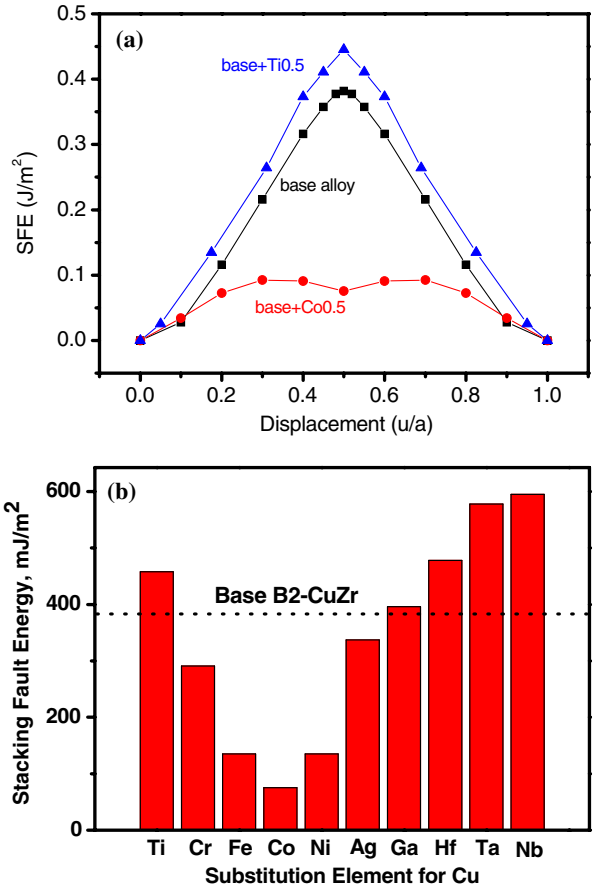

FIG. 1 (color online). Stacking fault energy on the (011)[100] slip system of the $B2$-CuZr phase and the ones with half of Cu on the slip plane substituted by Co or Ti (a), and the stacking fault energy of the $B2$-CuZr phase substituted with different elements (b).

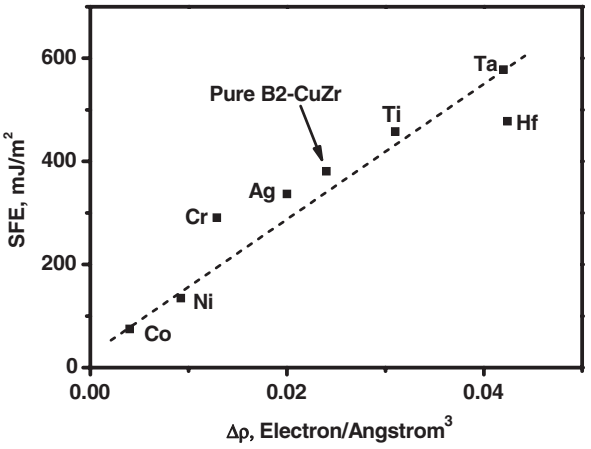

FIG. 2. The SFE values of the $B2$-CuZr phase doped with alloying elements as a function of the electronic density charge redistribution on the (011)[100] slip system.

that increases the electron charge density redistribution also enhances the SFE, which is consistent with the tendency in other alloy systems [30,31]. Notably, the Co substitution of Cu in the $B2$-CuZr structure drastically reduces the electron charge density redistribution from 0.024 to 0.004 electron/Å^3 during the stacking fault formation, thus decreasing the stacking fault energy. By contrast, the addition of Ti increases the electron charge density redistribution, thus increasing the SFE on the slipping plane of the $B2$ phase.

Generally, a lower SFE may facilitate deformation twinning to initiate and thus stimulates the martensitic transformation of the austenite $B2$ structure [13,33]. The onset temperature (M_s) and activation energy of the martensitic transformation in the $B2$ structures doped with different elements were measured by DSC at different cooling rates (an example of DSC curves at a cooling rate of 10 K/min was shown in Fig. S2; see the Supplemental Material in Ref. [32]). M_s was found to be cooling-rate dependent but at the same cooling rate of 10 K/min, the M_s value of the initial $B2$ is 337 K, while that of the $B2$ substituted with Ti and Co is 326 and 360 K, respectively. Clearly, the smaller the SFE the higher the M_s, confirming our hypothesis that proper alloying can facilitate the martensitic transformation. Similarly, the activation energy of the martensitic transformation of the $B2$ phase doped with different alloying elements shows the same trend with the SFE (see the related Kissinger plots for estimating the activation energy in Fig. S3 of the Supplemental Material in Ref. [32]); i.e., the Co addition reduced the activation energy from 85 to 74 kJ/mol while the Ti addition increase it up to 92 kJ/mol, further affirming that the lower SFE can facilitate the martensitic transformation and may give rise to different macroscopic mechanical behavior in these TRIP (transformation induced plasticity)-reinforced BMG composites upon loading.

To validate this hypothesis, several BMG composites reinforced by the $B2$-CuZr phases with different alloying elements were fabricated. In each composite sample, only a minor fraction of 0.5% of the alloying elements was added so that characteristics (e.g., size, volume fraction, and morphology) of the precipitated $B2$ phase and glass-forming ability of the amorphous matrix are not altered severely.

X-ray diffraction patterns (see Fig. S4 of the Supplemental Material in Ref. [32]) of the representative alloys, i.e., $Zr_{48}Cu_{48}Al_4$ (base alloy), $Zr_{48}Cu_{47.5}Al_4Ti_{0.5}$, and $Zr_{48}Cu_{47.5}Al_4Co_{0.5}$ alloys with a casting diameter of 3 mm, exhibit several similar sharp peaks, which were identified as the $B2$ phase, superimposed on a hump representative of glassy matrix, indicating that all composites consist of the single $B2$-CuZr phase embedded in the glassy matrix. SEM investigation further reveals that the $B2$ spherical particles have a similar fraction and morphology in these samples (see Fig. S5 in the Supplemental Material in Ref. [32]), confirming that minor additions of Co or Ti did not alter the glass-forming ability and the characteristics of the $B2$ precipitates in the glassy matrix. Nevertheless, the true tensile stress-strain curves of these three kinds of BMG composites show distinct differences, as demonstrated in Fig. 3. The base alloy exhibits an apparent yielding phenomenon and a tensile ductility of about 2%. The stress keeps almost constant after yielding and no notable work-hardening behavior was observed. With 0.5% Ti substituting Cu, the yield strength distinctly increases but the tensile ductility dramatically decreases, indicating an early development of plastic instability. For the alloy with 0.5% Cu replaced by Co, the sample yields at a relatively low stress but undergoes a pronounced work hardening after yielding. The tensile ductility reaches about 7% and the ultimate true strength is about 200 MPa higher than that of the base alloy, demonstrating that minor additions of Co can remarkably improve the tensile ductility and work-hardening capability of the present BMG composite.

To further understand the underlying mechanism, microstructure of these three composites was characterized using high resolution transmission electron microscopy (HRTEM). In both the base and Ti-containing alloys, in addition to the micrometer sized $B2$ particles, numerous nanocrystals indexed as the austenitic $B2$ structure are found [Fig. 4(a)], which is consistent with previous results [34]. In the Co-containing alloy, nevertheless, nanosized $B2$ crystals can also be observed but with a distinct characteristic [Fig. 4(b)]. From the blowup of a nanocrystal shown in Fig. 4(b), stacking faults and twin embryos were already formed. Based on the selected area diffraction (SAED), the crystallographic structure in the vicinity of the twin boundary was identified as the monoclinic $B19'$ structure [left inset in Fig. 4(d)], while the region away from the twin boundary was still $B2$-CuZr [right inset in Fig. 4(d)]. In other words, twinning embryos with the $B19'$ martensitic lattice have already nucleated in the rapid quenched Co-containing BMG composite. However,

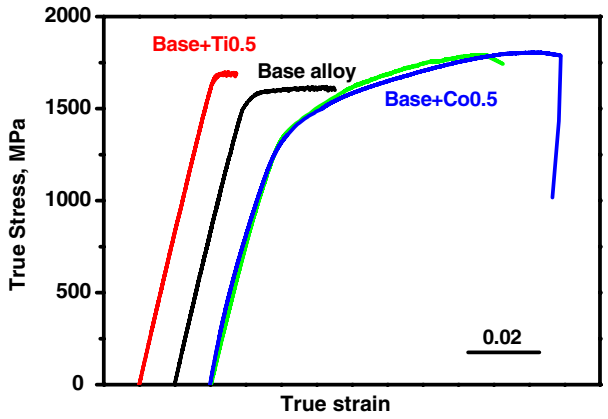

FIG. 3 (color online). True tensile stress-strain curves of the $Zr_{48}Cu_{48}Al_4$, $Zr_{48}Cu_{47.5}Al_4Co_{0.5}$, and $Zr_{48}Cu_{47.5}Al_4Ti_{0.5}$ BMG composites.

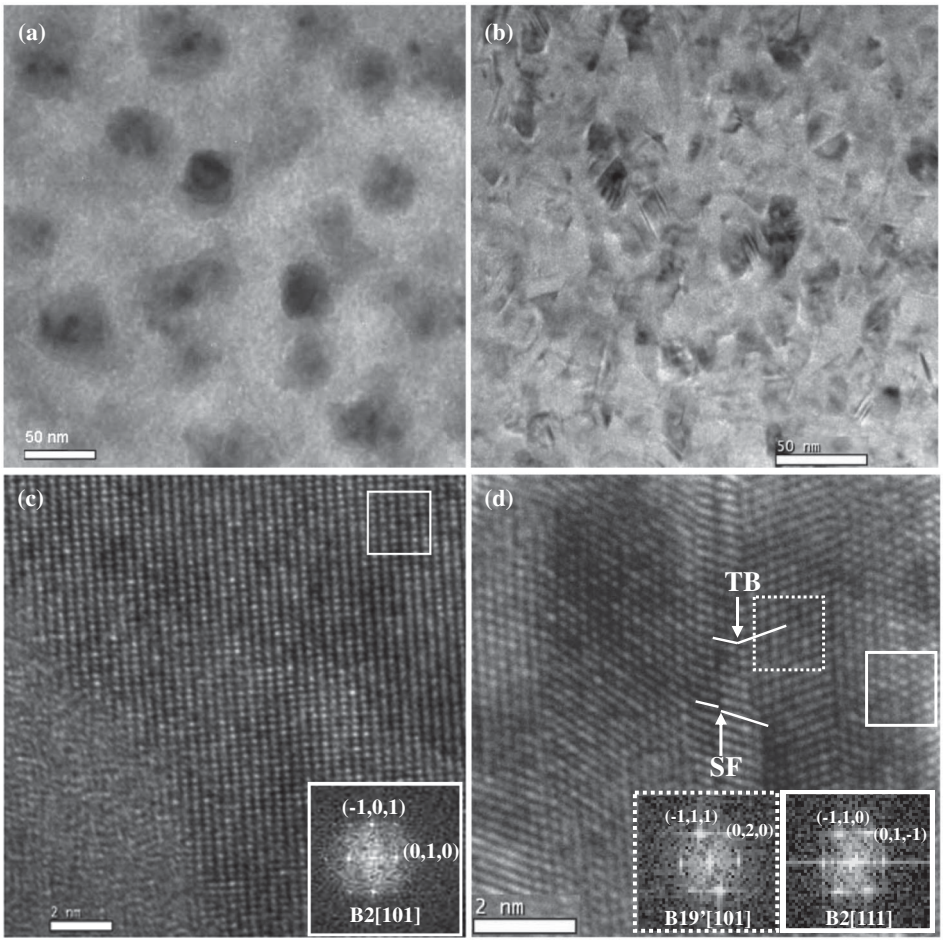

FIG. 4. HRTEM images of the $B2$ nanocrystals embedded in $Zr_{48}Cu_{48}Al_4$ (a) and $Zr_{48}Cu_{47.5}Al_4Co_{0.5}$ (b) BMG composites. (c) and (d) are the enlargement of a nanocrystal in (a) and (b), respectively. Insets are the SAED patterns corresponding to the circled area.

similar twinning nuclei were not seen in the other two alloys [see Fig. 4(c)]; this correlated well with our *ab initial* calculation shown in Fig. 1. It has been recognized that, kinetically, it is often easier to thicken a twin rather than to nucleate a fresh one [35,36]. Consequently, deformation twinning is relatively easy to be induced upon straining in the crystalline phase with 0.5% Cu replaced by Co because of the presence of the quenching-in twin nuclei formed during casting.

As expected, in the Co-containing specimens stretched about 3% ductility, extensive twinning is observed and twinned crystals expanded and coalesced to form the lath-shaped structures (see Fig. S6 in the Supplemental Material in Ref. [32]). Apparently, the initially quenched-in twinning nuclei gradually developed by consuming the surrounding matrix, and the deformation twinning proceeds continuously upon tension and finally gets coagulated to form large martensitic plates (Fig. S6 in the Supplemental Material in Ref. [32]). These martensitic laths could have different orientations, which are beneficial for accommodating the applied strain and alleviating the local stress concentration effectively [37].

Therefore, it can be clearly seen that macroscopic deformation behavior of TRIP-reinforced BMG composites can be significantly optimized by tailoring SFE of the reinforced austenitic phase. Thus, a more realistic alloying guideline for tailoring SFE and its relation with macroscopic mechanical behavior was urgently in demand. By systematically investigating physical factors that may affect SFE of $B2$-CuZr, it is found that both the electronegativity and the atomic radius difference between the doped element and substituted element correlate closely with the SFE of the doped $B2$ structure, as demonstrated in Fig. 5. Clearly, a smaller electronegativity and atomic radius difference between the doping element and Cu give rises to a lower SFE of the doped $B2$-CuZr phase. Therefore, a general guideline for selecting suitable alloying elements to tailor the SFE of the $B2$ phase was obtained, which is important for manipulating the martensitic transformation behavior of $B2$ in general. As a result, the martensitic transformation of the $B2$ crystals doped with suitable elements that reduce the SFE could occur much easier, which eventually leads to an earlier yielding, a larger plasticity, and more pronounced work-hardening capability.

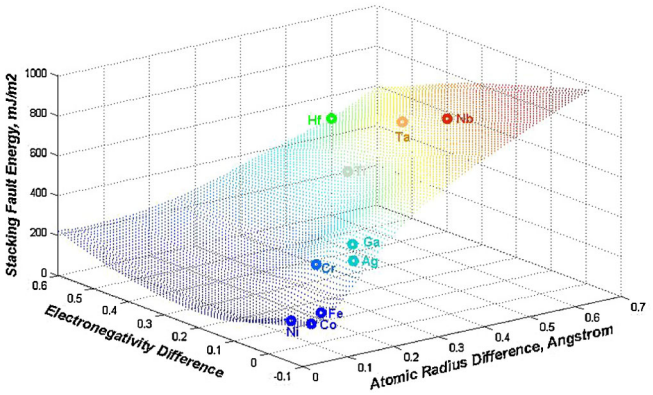

FIG. 5 (color online). Dependence of the stacking fault energy of the doped $B2$ phase on the eletronegativity and radius difference between the doping and substituted elements.

In conclusion, martensitic transformation of the austenitic phases has been introduced into BMG materials as an effective mechanism to enhance ductility and work-hardening capability. The potency of deformation twinning of the reinforcing phase can be tailored by altering the SFE through minor alloying additions. Specifically, the alloying addition must have the electronegativity value and atomic size that are similar to the element in the $B2$ phase it replaces. *In situ* formed $B2$ crystals with a lower SFE facilitates deformation twinning and phase transformation, and consequently improved the tensile performance of the BMG composites. The implications of this study are important for developing high-performance BMG composites in the other alloy systems.

This research was supported in part by the National Natural Science Foundation of China (No. 51010001 and No. 51001009), 111 Project (B07003), and Program for Changjiang Scholars and Innovative Research Team in University. One of the authors (Y. W.) acknowledges the financial support from "the Fundamental Research Funds for the Central Universities."

*luzp@ustb.edu.cn

[1] W. L. Johnson, MRS Bull. **24**, 42 (1999).
[2] A. Inoue, Acta Mater. **48**, 279 (2000).
[3] M. W. Chen, Annu. Rev. Mater. Res. **38**, 445 (2008).
[4] C. A. Schuh, T. C. Hufnagel, and U. Ramamurty, Acta Mater. **55**, 4067 (2007).
[5] D. C. Hofmann, J.-Y. Suh, A. Wiest, G. Duan, M.-L. Lind, M. D. Demetriou, and W. L. Johnson, Nature (London) **451**, 1085 (2008).
[6] D. C. Hofmann, J.-Y. Suh, A. Wiest, M.-L. Lind, M. D. Demetriou, and W. L. Johnson, Proc. Natl. Acad. Sci. U.S.A. **105**, 20136 (2008).
[7] S. Pauly, J. Das, J. Bednarcik, N. Mattern, K. B. Kim, D. H. Kim, and J. Eckert, Scr. Mater. **60**, 431 (2009).
[8] C. P. Kim, Y. S. Oh, S. Lee, and N. J. Kim, Scr. Mater. **65**, 304 (2011).
[9] Y. Wu, Y. H. Xiao, G. L. Chen, C. T. Liu, and Z. P. Lu, Adv. Mater. **22**, 2770 (2010).
[10] Y. Wu, H. Wang, H. H. Wu, Z. Y. Zhang, X. D. Hui, G. L. Chen, D. Ma, X. L. Wang, and Z. P. Lu, Acta Mater. **59**, 2928 (2011).
[11] D. C. Hoffman, Science **329**, 1294 (2010).
[12] S. W. Seo and D. Schryvers, Acta Mater. **46**, 1165 (1998).
[13] S. Pauly, G. Liu, S. Gorantla, G. Wang, U. Kühn, D. H. Kim, and J. Eckert, Acta Mater. **58**, 4883 (2010).
[14] K. Lu, L. Lu, and S. Suresh, Science **324**, 349 (2009).
[15] X. L. Wu, Y. T. Zhu, Y. G. Wei, and Q. Wei, Phys. Rev. Lett. **103**, 205504 (2009).
[16] Y. H. Zhao, Y. T. Zhu, X. Z. Liao, Z. Horita, and T. G. Langdon, Appl. Phys. Lett. **89**, 121906 (2006).
[17] E. Ma, Y. M. Wang, Q. H. Lu, M. L. Sui, L. Lu, and K. Lu, Appl. Phys. Lett. **85**, 4932 (2004).
[18] G. Kresse and J. Hafner, Phys. Rev. B **49**, 14251 (1994).
[19] G. Kresse and J. Furthmüller, Comput. Mater. Sci. **6**, 15 (1996).
[20] P. E. Blöchl, Phys. Rev. B **50**, 17953 (1994).
[21] G. Kresse and D. Joubert, Phys. Rev. B **59**, 1758 (1999).
[22] J. P. Perdew and Y. Wang, Phys. Rev. B **45**, 13244 (1992).
[23] K. Momma and J. Izumi, J. Appl. Crystallogr. **41**, 653 (2008).
[24] J. Izumi and K. Momma, Solid State Phenom. **130**, 15 (2007).
[25] J. A. Yan, C. Y. Wang, and S. Y. Wang, Phys. Rev. B **70**, 174105 (2004).
[26] X. Z. Wu, R. Wang, S. F. Wang, and Q. Y. Wei, Appl. Surf. Sci. **256**, 6345 (2010).
[27] N. Hatcher, O. Y. Kontsevoi, and A. J. Freeman, Phys. Rev. B **80**, 144203 (2009).
[28] A. Froseth, H. V. Swygenhoven, and P. M. Derlet, Acta Mater. **52**, 2259 (2004).
[29] D. Q. Zhou, Y. Wu, and Z. P. Lu (unpublished).
[30] S. Ogata, J. Li, and S. Yip, Science **298**, 807 (2002).
[31] Y. Qi and R. K. Mishra, Phys. Rev. B **75**, 224105 (2007).
[32] See Supplemental Material at http://link.aps.org/supplemental/10.1103/PhysRevLett.109.245506 for experimental details and Figs. S1–S6.
[33] X. Q. Wang, Phys. Rev. B **78**, 092103 (2008).
[34] S. Pauly, S. Gorantla, G. Wang, U. Kühn, and J. Eckert, Nature Mater. **9**, 473 (2010).
[35] S. Ogata, J. Li, and S. Yip, Phys. Rev. B **71**, 224102 (2005).
[36] M. W. Chen, E. Ma, K. J. Hemker, H. W. Sheng, Y. M. Wang, and X. M. Cheng, Science **300**, 1275 (2003).
[37] T. Waitz, Acta Mater. **53**, 2273 (2005).